JOURNAL OF SOLID STATE CHEMISTRY 68, 153–162 (1987)

Characterization of Fine Particles of the α-Fe_2O_3–SnO_2 System with Residual SO_4^{2-} Ions on the Surface

M. TAKANO* AND Y. BANDO
Institute for Chemical Research, Kyoto University, Uji, Kyoto-fu 611, Japan

N. NAKANISHI

Faculty of Science, Konan University, Kobe 658, Japan

AND M. SAKAI AND H. OKINAKA

Wireless Research Laboratory, Matsushita Electric Industrial Company, Ltd., 1006 Kadoma, Osaka 571, Japan

Received April 28, 1986

The α-Fe_2O_3–SnO_2 system in fine powder form prepared by thermal decomposition at 873 K of precursory oxide hydroxides and containing a few weight percent of residual SO_4^{2-} ions on the surface has been characterized by X-ray diffraction, by the ^{57}Fe and ^{119}Sn Mössbauer effects, and by other techniques. A certain α-Fe_2O_3-rich composition of this system has been used practically as an excellent but cheap CH_4 sensor as a city gas-leak alarm. Fine particles of generally $\lesssim 10^3$ nm^3 with intermediate compositions remain far from the equilibrium state in the aspect that the solubility is drastically widened for both α-Fe_2O_3 and SnO_2, especially for the latter: solid solutions $(Fe_2O_3)_{1-x}(SnO_2)_x$ with $x \lesssim 0.2$ crystallizing in the corundum-type structure and with $x \gtrsim 0.7$ crystallizing in the rutile-type structure seem to be formed. The SO_4^{2-} ions may be considered to form microscopic cages around fine particles which, although being thermodynamically unstable, are nevertheless practically stable for more than a few years at the operating temperature of 673 K as demonstrated by the practical use as a sensor. A rapid separation into and a rapid particle growth of α-Fe_2O_3 and SnO_2 are brought about by thermal release of the SO_4^{2-} ions at 1073 K.

Introduction

It was found recently that the electrical resistivity of a loosely sintered fine powder of α-Fe_2O_3 dropped when the body came in contact with combustible gases such as hydrogen, methane, ethyl alcohol, and isobutane (*1*). An excellent city gas-leak alarm monitoring CH_4 content in the air by the resistivity change at 673 K has come onto the market. The fine powder was obtained by thermal decomposition of precipitates formed by adding aqueous ammonia to a solution containing Fe^{3+} ions, a small amount of additive quadrivalent cations such as Ti^{4+}, Sn^{4+}, or Zr^{4+}, and the counteranions SO_4^{2-} and Cl^-. The ferric oxide powder thus formed contains not only the nonvolatile metal additive but also a few weight percent of SO_4^{2-} ions on the surface even after the final sintering treatment at

* Author to whom correspondence should be addressed.

0022-4596/87 $3.00

873 K for 1 hr. Both the metal additive and the residual SO_4^{2-} ions have been found to be important for improvement of the gas-detecting function including factors not only of the magnitude of the resistivity drop but also of the response time, gas selectivity, and lifetime.

As for the mechanism of the resistivity change, formation of Fe^{2+} ions providing hopping electrons by surface reduction was suggested for gases other than methane, while some kind of electron exchange with the oxide surface on adsorption was suggested for the less combustible methane. Both the quadrivalent cations and the residual SO_4^{2-} ions seem to "activate" α-Fe_2O_3 which is by nature a very stable oxide. This activation has been claimed to be closely related to poor crystallization of the chemically modified powder (*1*).

To characterize the activated powder from the view point of solid state chemistry, we have applied various techniques, and this paper reports mainly the results of X-ray diffraction (XRD) and the Mössbauer effect (ME) measurements. Samples from the α-Fe_2O_3–SnO_2 system covering the whole composition range were used. The ME was measured on both ^{57}Fe and ^{119}Sn to acquire complementary information. From the collected data, the composition dependence of the crystalline form and the distributions of the Fe^{3+} and Sn^{4+} ions have been investigated. As a result, this composite fine powder system has been found to be in a state far from that at thermal equilibrium state; the presence of the residual SO_4^{2-} ions contributed toward the maintenance of the unstable state during the manufacturing heat treatment at 873 K, and for more than a few years at the operating temperature of 673 K.

Experimental

The samples were fabricated as follows (*1*). Homogeneous aqueous solutions containing appropriate amounts of Fe^{3+}, Sn^{4+}, SO_4^{2-}, and Cl^- were prepared. Then, aqueous ammonia was added to the solutions to increase the pH to 8. The hydrolysis products were filtered, washed with distilled water, dried at 373 K, and thermally decomposed at 673 K. Resistivity measurements were made at 673 K on cylinders sintered at 873 K for 1 hr in air. In each specimen two platinum lead wires were embedded before sintering. The porosity was typically 60%. Further details of the sample preparation and resistivity measurements are given elsewhere (*1*). Samples for measurements of XRD, transmission electron microscopy (TEM), and the ME were treated in air in powder form under various conditions with respect to temperature and time.

The specific surface area was measured by the BET method using nitrogen. The content of the residual SO_4^{2-} ions was estimated thermogravimetrically on heating the sample powder above 1073 K for release of SO_3. XRD was measured with Rigaku RU-200 apparatus equipped with a graphite monochrometer. Cu$K\alpha$ radiation was used. The ME was measured using ^{57}Co/Rh and $Ca^{119}SnO_3$ sources. Metallic iron, $CaSnO_3$, and metallic tin were used as control samples for velocity calibration and as the isomer shift references. For TEM observation, a JEM-100CX was used.

Results and Discussion

i. Samples Treated at 873 K

Figure 1 shows the dependences of the specific surface area, the amount of SO_4^{2-} ions, and the CH_4 sensitivity at 673 K on SnO_2 content for samples treated at 873 K for 1 hr in air. The gas sensitivity is expressed by $R_{a(0)}/R_{g(0.5)}$, where $R_{g(0.5)}$ stands for the resistivity in air containing 0.5 vol% of methane and $R_{a(0)}$ for the resistivity in air without methane. All of these measured values reach maxima at SnO_2 = 15 ~20 mole%. The decrease in sensitivity with in-

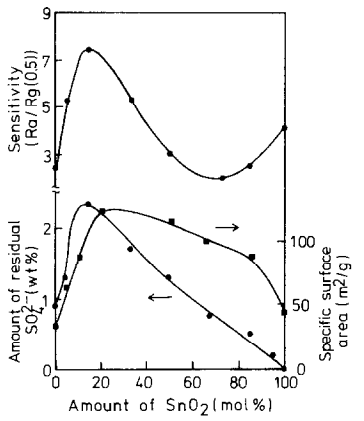

FIG. 1. The specific surface area, the amount of residual SO_4^{2-} ions, and the CH_4 sensitivity at 673 K are plotted against the SnO_2 content. The samples were treated at 873 K for 1 hr.

creasing SnO_2 content beyond the optimum composition is much sharper than that in specific surface area. This seems to manifest the importance of the Fe^{3+} and SO_4^{2-} ions which decrease with increasing SnO_2 content.

Figure 2 shows the XRD patterns. Samples are given notations, e.g., 5-873, indicating their SnO_2 contents in mole percent and final heat treatment temperatures. The pattern for the sample containing no SnO_2 is typical of α-Fe_2O_3 crystallizing in the corundum structure, and is indexed on the basis of the hexagonal cell. Addition of SnO_2 broadens the peaks. It is characteristic that those peaks with indices (hkl) with $l = 2$, 4, and 8 are broader than those of $l = 0$, 3, and 6. For example, the peak widths of (104) and (110) correspond to crystallite sizes of about 50 and 150 Å, respectively, for sam-

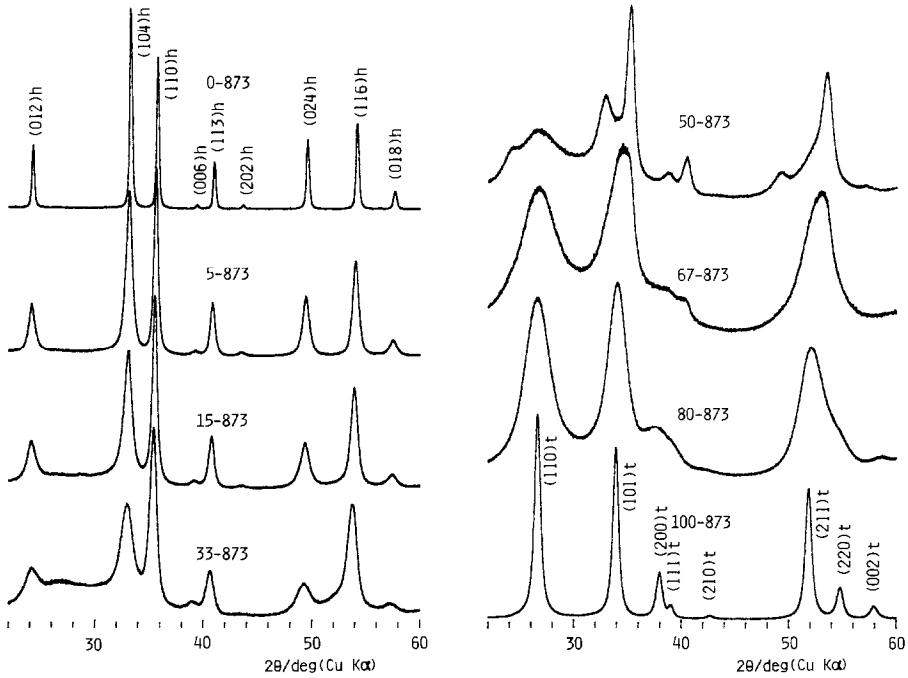

FIG. 2. XRD patterns for samples treated at 873 K for 1 hr. The sample notations indicate SnO_2 contents in mole percent and heat treatment temperatures. The peaks for α-Fe_2O_3 (0-873) and SnO_2 (100-873) are indexed on the basis of the hexagonal corundum cell $(hkl)_h$, and the tetragonal rutile cell $(hkl)_t$, respectively.

ple 33-873. This type of inhomogeneous broadening is known to occur even for pure α-Fe_2O_3 prepared by low-temperature decomposition of α-FeOOH (*2*). Watari *et al.* (*2*) interpreted this as a morphological effect due to the twin formation in the process of topotactic dehydration transformation. The Fe^{3+} ions in α-Fe_2O_3, which occupy two-thirds of the octahedral voids of the oxygen *hcp* lattice, may be considered to form two-dimensional honeycomb lattices stacked along the hexagonal *c* axis like *abcabc* . . . . The obverse and reverse twin components have the common oxygen *hcp* lattice but have different cation stacking sequences of *abcabc* . . . for one component and *acbacb* . . . for the other. The $l \neq 3n$ reflections belonging to either the obverse or reverse variant are seriously broadened because of the very small component size, while the $l = 3n$ peaks common to both twin components remain sharp because of coherency at the twin boundary. However, this argument does not exactly apply to the present system. The precursory oxidehydroxide changes from the γ-FeOOH type having an *fcc* oxygen lattice to the α-FeOOH type having an *hcp* oxygen lattice only for $SnO_2 \geq 15$ mole% and, moreover, we detected dissolution of an unexpectedly large amount of Sn^{4+} ions, and hence the accompanying metal vacancies formed for charge compensation into the α-Fe_2O_3 lattice.

The dissolution causes a change in the lattice constants as detected by XRD. Both the *a* and *c* axes of the hexagonal corundum cell are elongated with increasing SnO_2 content at an approximate rate of 0.02%/SnO_2 mole% for $SnO_2 \leq 50$ mole%. However, the dissolution is not homogeneous and nucleation of the rutile-type phase begins for $SnO_2 \geq 15$ mole%: the seriously broadened (110) peak of the rutile structure, which might be mistaken as a slightly swollen baseline, appears at $2\theta \sim 27$. This peak tends to grow and sharpen on prolonging the final heat treatment or raising the temperature, suggesting that the rutile-type phase is formed by thermally stimulated coagulation of the Sn^{4+} ions once dissolved in the corundum structure more homogeneously. The above-mentioned selective broadening of the XRD peaks may be partly ascribed to the precipitation process of the rutile-type phase. Precursory clustering of Sn^{4+} ions and accompanying vacancies or further advanced precipitation of the rutile-type phase would destroy the coherency in the cationic lattice of the corundum structure, while the oxygen lattice would remain coherent more easily because the oxygen lattice in the rutile structure is fundamentally *hcp* as in α-Fe_2O_3. For compositions of $SnO_2 \geq 67$ mole%, the rutile-type pattern becomes dominant. The *a* axis of the tetragonal cell shrinks with increasing SnO_2 content at a rate of $\sim$0.02%/SnO_2 mole%, while the *c* axis lengthens at a rate of $\sim$0.08%/SnO_2 mole%, suggesting the dissolution of α-Fe_2O_3 into SnO_2.

The ME spectra measured at 4 K are shown in Fig. 3. These are useful for the purpose of studying the distribution of the Fe^{3+} and Sn^{4+} ions, since extra peak broadening at higher temperatures, e.g., 300 and 77 K, due to the superparamagnetic nature of the sample fine powders is eliminated. As for the ^{57}Fe spectra, both the magnetic hyperfine field (H_i) and the isomer shift (*IS*) are characteristic of the valence state of 3+ for all the compositions. The six-finger magnetic hyperfine pattern for sample 5-873 has parameters of $IS = 0.49$ mm/sec $H_i = 53$ T, and a quadrupole splitting (*QS*) of $QS = 0.44$ mm/sec, where *QS* corresponds to $S_1 - S_2$ given in Fig. 3. It is well-known that α-Fe_2O_3 undergoes a spin flip transition, the so-called Morin transition, at 260 K, where the spin axis changes from within the *c* plane to parallel to the *c* axis. This transition appears in the ME spectrum as a change in *QS* from $\approx +0.4$ mm/sec above 260 K to ≈ -0.8 mm/sec below. The transi-

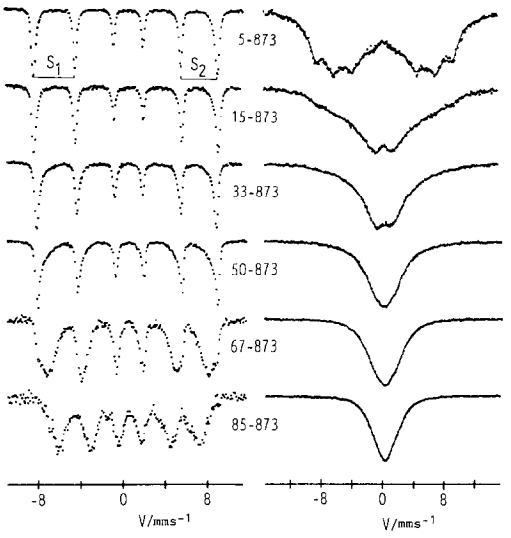

FIG. 3. Mössbauer spectra at 4 K of samples treated at 873 K for 1 hr. For each sample, the ^{57}Fe and ^{119}Sn spectra are shown on the left and on the right, respectively.

tion temperature is known to decrease or vanish if α-Fe_2O_3 is contaminated with impurities such as Sn^{4+} or Ti^{4+} (*3*) or if the particle size is decreased (*4*). The positive *QS* value for the present sample indicates that the Morin transition is absent because of the cooperative effect of particle size and impurity. This situation holds also for the other compositions. For the composition of SnO_2 = 50 mole%, a broadened magnetic pattern with an approximate average H_i of 46 T is superimposed. This component can be obscurely seen also for sample 33-873, while it becomes dominant for sample 67-873. Considering the appearance of the broadened rutile-type XRD peaks for SnO_2 $\geq$ 15 mole%, it is reasonable to assume that the Fe^{3+} ions dissolved in SnO_2 give this broadened magnetic hyperfine pattern. The H_i for the composition of SnO_2 = 85 mole% is further decreased to about 42 T, probably because the Néel temperature is decreased to not much above 4 K for the low Fe^{3+} concentration.

The *IS* of about 0.1 mm/sec vs $CaSnO_3$ indicates that tin takes the valence state of Sn^{4+} for every composition studied. Though a Sn^{4+} ion itself is nonmagnetic, its nucleus feels a nonvanishing magnetic hyperfine field by the effect of a supertransferred hyperfine interaction (STHFI) with the Fe^{3+} ions in its vicinity. This is a short-ranged cation–cation spin transfer via molecular orbitals involving Fe^{3+} : 3*d*, Sn^{4+} : 5*s*, and O^{2-} : 2*p* (*5*). The spectrum for sample 5-873 shows a well-resolved six-finger pattern the supertransferred hyperfine field (STH_i) of which reaches 13 T. This value coincides with the literature value for α-Fe_2O_3 containing $^{119}Sn^{4+}$ ions as a dilute impurity (*6, 7*). The present spectrum is, however, more complex, reflecting inhomogeneity of the surroundings of the Sn^{4+} ions due to the high content. The induced distribution in STH_i was estimated in the form of a histogram by computer fitting, when the Lorentzian line shape was assumed. The results together with those for the other compositions are shown in Fig. 4. In the histogram for sample 5-873 it is evident that the STH_i takes a wide range of values with four well-defined peaks at 13, 10, 6, and 2 $\sim$ 3 T. With increasing SnO_2 content, the experimental spectrum tends to show a more enhanced absorption at the central part. The histogram shows this tendency as an increase of Sn^{4+} ions feeling a STH_i of less than 5 T.

Figure 5 illustrates the idealized cation distribution in α-Fe_2O_3 viewed along the *c* axis, where slight displacements of the atomic positions in the real structure are neglected. As for the magnetic structure, Fe^{3+} ions in one honeycomb lattice have parallel magnetic moments, while those in adjacent lattices have antiparallel moments. This results from strong interlattice antiferromagnetic superexchange interactions, for example, between the Fe^{3+} ion located at the $\circ$0 site (see Fig. 5) and the nine situated at sites $\triangle$1 $\sim$ 6 and $\triangledown$2, 4, and 6 (*8*). Sn^{4+} ions incorporated into α-Fe_2O_3

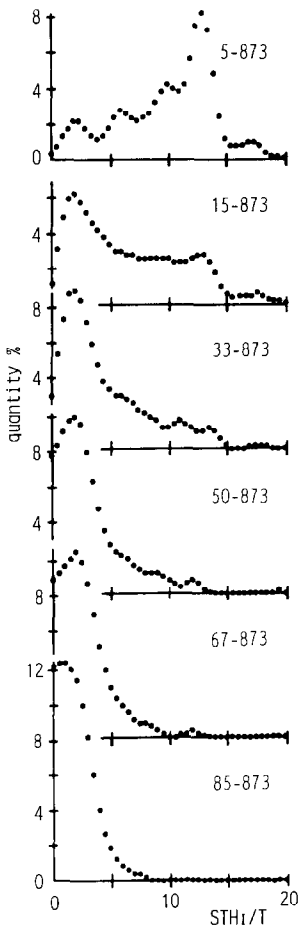

FIG. 4. Histograms of the supertransferred hyperfine field at 4 K of $^{119}Sn^{4+}$ in various compositions. The corresponding spectra are shown in Fig. 3.

are expected to substitute at the Fe^{3+} sites. Here, we suppose that one of them is located at site ∘0. There are 13 neighboring cation sites around it. The density and sign of transferred spin depend both on the nature of the molecular orbital involving the surrounding cations and anions and on the magnetic structure. If all the neighboring sites are occupied by Fe^{3+} ions, the STH_i amounts to 13 T. It is possible to classify the neighboring cation sites into three groups by their anticipated contributions to the STH_i (*7*). The first group includes the △1 ~ 6 and ▽2, 4, and 6 sites. The bondings between site ∘0 and these are almost equivalent as judged crystallographically, and the Fe^{3+} ions of this group have parallel spins. The second group includes sites ∘1, 3, and 5 for similar reasons. These two groups have opposite spins. The third group includes only the ▽0 site. The second and third groups are located nearer to site ∘0 via deeply bent metal–oxygen–metal bonds. If these are partially substituted by Sn^{4+} ions and/or vacancies formed for charge compensation, the value of STH_i at the ∘0 site would change variously depending on the distribution of the substituted sites. A vacancy acts, in effect, as a nonmagnetic metal ion. If the concentration of Sn^{4+} ions is as high as $Fe^{3+} : Sn^{4+} = 38 : 1$ as in sample 5-873, then the possibility of one-site substitution is very high. The most probably substituted is group 1, including the furthest and the most sites: the long distance is favorable for a cation but not for a vacancy. So, the second highest peak at 10 T in the histogram can be assigned to this case. Being separated regularly by about 3.5 T, the third and fourth peaks at 6 and 2.5 T may also be assigned to a double and triple substitution, respectively. However, the probabilities calculated on the basis of random substitution are much lower. This suggests in turn that Sn^{4+} ions and vacancies tend to gather as may well be expected from the very low solubility of SnO_2 into α-

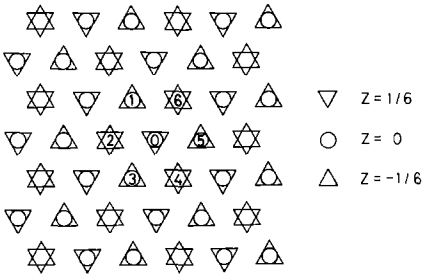

FIG. 5. Idealized distribution of the cation sites in the corundum structure. Three honeycomb lattices at $z = 0, \pm\frac{1}{6}$ are stacked.

Fe_2O_3 in the thermal equilibrium state at 873 K to be shown later.

By the way, the reduction in STH_i of 3.5 T per substituted site means in turn that the nine Fe^{3+} ions of group 1 create a total STH_i of 31.5 T. The opposite contribution to reduce this value to 13 T must be made mainly by the group 2 ions. The small peak at 17.5 T in the histogram may correspond to the ◦0 site Sn^{4+} ion accompanied with one substituted group 2 site. If so, the contribution by one group 2 Fe^{3+} ion amounts to −4.5 T. This leads to a likewise negative contribution by the ▽0 site Fe^{3+} ion of −5 T.

The peaks in the histogram are considerably broadened for the occurrence of many more complicated arrangements of Sn^{4+} ions and vacancies not only at the near neighboring sites but also at further ones. The broadening becomes more serious and the most important peak becomes located at ≤2 T, with increasing SnO_2 content. Especially for 67-873 and 85-873 which have the rutile-type structure the STH_i's are almost limited to 5 T. In case that α-Fe_2O_3 saturated with SnO_2, and SnO_2 saturated with α-Fe_2O_3 coexist at intermediate compositions, two kinds of histograms corresponding to the different phases must be superimposed with various ratios. The composition dependence of the experimental histogram is, however, rather particular, thus indicating that further dissolution and precipitation of the second phase proceed at the same time at the intermediate compositions. This is consistent with the XRD results described already.

There remains a remote but disputable contrary possibility that the line broadening which has been attributed to small STH_i's of <5 T is due to a quadrupole interaction. This was examined by ME measurements at intermediate temperatures. For example, the ^{57}Fe spectra of sample 67-873 showed superparamagnetic behavior with a blocking temperature of about 40 K. Correspondingly, the ^{119}Sn spectra became broader below this temperature, confirming our attributing the broadening to STHFI: the STH_i is limited to 5 T for structural and compositional reasons.

The XRD and ME results described above have revealed consistently that α-Fe_2O_3 and SnO_2 remain dissolved in each other over a wide composition range on either side after annealing for 1 hr at 873 K. Though it is not possible to determine the solubility limits exactly because of the inhomogeneous nature, compositions of $0.8Fe_2O_3$–$0.2SnO_2$ with the corundum structure and $0.3Fe_2O_3$–$0.7SnO_2$ with the rutile structure seem to exist under these conditions. These are surprizingly high solubilities in comparison with the thermodynamical equilibrium state, which will be described in the following section.

ii. The α-Fe_2O_3–SnO_2 System in the Thermal Equilibrium State

The purpose of this section is to estimate approximately the solubility limit of the α-Fe_2O_3–SnO_2 system in its thermal equilibrium state. To our knowledge, the phase diagram of this system was reported by Cassedanne (*9*) only for above 1473 K.

A new series of samples were prepared by the usual ceramic method from fine powders of α-Fe_2O_3 and SnO_2, both having a nominal purity of 99.99% (Furuuchi Chemical Co.). These raw materials were mixed at various ratios, pressed into disks, fired at 1273 K for 24 hr in air, and quenched. These pellets were then crushed, mixed and pressed, and heated at 1473 K in air for more than 240 hr. The products were quenched into ice water. Each composition was divided into several parts, which were subsequently annealed at different temperatures below 1473 K in air for 240 hr and then quenched into ice water. Samples thus obtained were subjected to XRD and the ME measurements. For brevity, only the results for treatments at 1473 and 1073 K

will be reported here. Figure 6 compares the ^{119}Sn spectra for samples C5-1473 and C5-1073 at room temperatures and also shows the ^{57}Fe spectrum for sample C95-1473 at room temperature, where the notation indicates the ceramic method of preparation, SnO_2 content in mole percent, and the final treatment temperature. XRD confirmed the absence of any phase other than the corundum or rutile structure. The spectrum of C5-1073 consists of magnetically perturbed and unperturbed absorptions with a relative intensity of approximately 12 : 5. The former, being split by a STH_i of 13 T, comes from Sn^{4+} ions dissolved in the lattice of α-Fe_2O_3, while the latter corresponds to a SnO_2-rich phase. Annealing at 1073 K exsolved the dissolved Sn^{4+} ions so that the magnetically perturbed component almost vanished. It is evident that the solubility of SnO_2 in α-Fe_2O_3 is 1 mole% or less at 1073 K, while it increases to 4 mol% at 1473 K. The ^{57}Fe ME spectrum for sample C95-1473 consists of a magnetic pattern of the α-Fe_2O_3 type only. A paramagnetic spectrum expected from Fe^{3+} ions dissolved in SnO_2 could not be found within experimental error. The solubility seemed to be less than 1 mole% even at 1473 K. Consistent results were obtained also by the XRD measurements. Further details will be published elsewhere.[1]

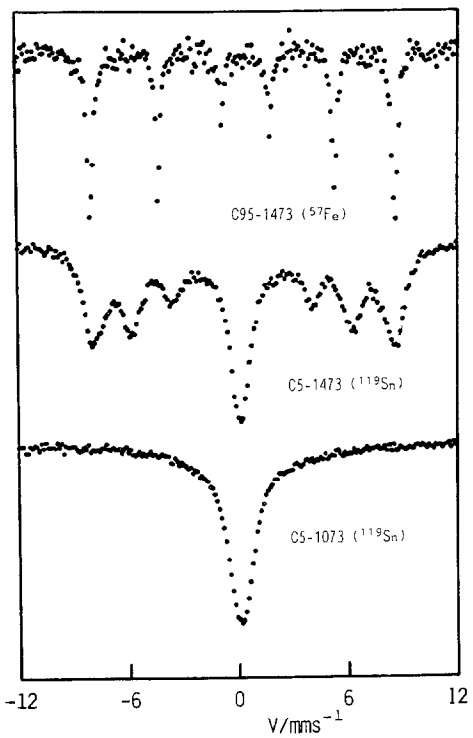

FIG. 6. ME spectra for samples in the thermal equilibrium state. The notations indicate the ceramic preparation method, SnO_2 contents in mole percent, and the final heat treatment temperatures.

The samples studied in the previous sections showing very broad solubility ranges may, thus, be considered to remain far from the equilibrium state. It is important from the viewpoint of the practical use as a gas sensor that the unusual state for the extremely fine powders can be retained for more than a few years at the operating temperature of 673 K.

iii. The Effects of the Residual SO_4^{2-} Ions

According to a previous paper (*1*), the residual SO_4^{2-} ions are released at composition-dependent temperatures below 1073 K. The release was detected by thermogravimetric and differential thermal analyses (TG-DTA) as a weight loss accompanied by an endothermic DTA peak. An exothermic peak following the endothermic peak was accompanied by narrowing of the XRD peaks and this was ascribed to "crystallization" of the oxide powder. In this section we report a further study on this phenomenon which would serve for the purpose of clarifying the role of the residual SO_4^{2-} ions.

Those samples reported in Section *i* were treated in air at 1073 K for 1 hr. Figure 7 compares samples 33-873 and 33-1073 ob-

[1] Cassedanne (*9*) reported much broader solubility ranges on both sides above 1473 K, which were determined from the composition dependence of specific gravity. The method applied in the present work is more microscopic and direct.

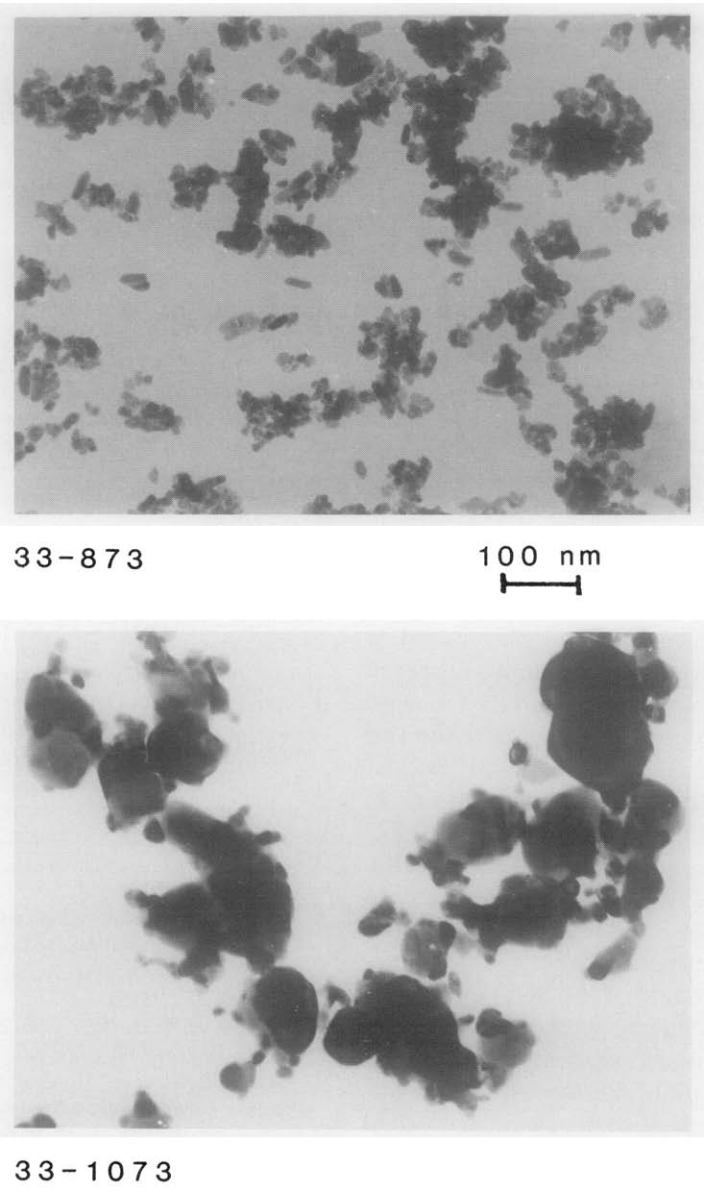

FIG. 7. Particles observed by TEM before (33-873) and after (33-1073) the heat treatment at 1073 K for removing the SO_4^{2-} ions.

served by TEM. The particles treated at the lower temperature look like homogeneous lean grains, while sample 33-1073 consists of comparatively large thin particles to which smaller stocky ones adhere. The latter sample was subjected to a microscopic compositional analysis with a JEM-200FX electron microscope equipped with an EDS system allowing analysis within an area of 10^2 nm^2. As a result it was found that iron and tin are contained separately in the larger and smaller particles, respectively: an almost complete separation into α-Fe_2O_3 and SnO_2 was suggested. This type of phase

separation accompanied with particle growth was observed for all the samples from 5-1073 to 95-1073 by XRD and for the ME. For example, the Morin transition was recovered in the purified and grown α-Fe_2O_3 particles as judged from the ^{57}Fe spectra at 4 K and the STHFI effects disappeared from the ^{119}Sn spectra at 4 K. These results consistently indicate that the thermal SO_4^{2-} release makes the original, mutually well-dissolved state unsettled. The temperature is high enough to allow a quick shift to the thermal equilibrium state characteristic of the α-Fe_2O_3–SnO_2 system.

We can schematically consider the residual SO_4^{2-} ions to form a microscopic cage in which an oxide particle in an unusual state is trapped. This is substantiated also by comparison with the behavior of samples prepared by using ferric nitrate instead of the sulfate. Two kinds of samples prepared from the different raw materials but with the same SnO_2 content of 33 mole% showed rather similar XRD patterns and ^{119}Sn ME spectra when these were treated at 673 K for 1 hr, but after a further treatment at 873 K for 1 hr the samples prepared from the nitrate showed a pronounced separation into α-Fe_2O_3 and SnO_2 in the XRD and ME properties. These observations seem to emphasize that the role of the SO_4^{2-} ions is not to create the unusual well-dissolved state but to suppress the separation. Once the cage is thermally broken, even atomic diffusion beyond the particle boundary would be accelerated by the repulsive tendency between the Fe^{3+} and Sn^{4+} ions and also by an increase in surface energy on the SO_4^{2-} release. It is interesting to note that the dynamical process of the separation and particle growth can be observed more easily by treating sample powders at lower temperatures: the XRD pattern changing with annealing time at 923 K extending to hundreds of hours reported in Ref. (*1*) suggests a considerable slowing down of the SO_4^{2-} release and the disproportionation into α-Fe_2O_3 and SnO_2. Further work on this subject is under progress.

Acknowledgments

The authors express the hearty thanks to Professor T. Takada for encouragement and to Mr. Y. Ikeda and Mr. T. Fujii for their technical service.

References

1. Y. Nakatani and M. Matsuoka, *in* "Proceedings of the 1st Sensor Symposium of the Institute of Electrical Engineers of Japan, Tokyo, 1981," p. 63; Y. Nakatani and M. Matsuoka, *Japanese J. Appl. Phys.* **21,** L758 (1982); and Y. Nakatani, M. Sakai, and M. Matsuoka, *in* "Proceedings of International Meeting of Chemical Sensors, Fukuoka, 1983," (Eds), p. 147, T. Seiyama, K. Fueki, J. Shiokawa, and S. Suzuki, Kodansha Ltd., Tokyo, and Elsevier, Amsterdam/New York (1983).
2. F. Watari, J. Van Landuyt, P. Delavignette, S. Amelinckx, and N. Igata, *Phys. Status Solidi A* **73,** 215 (1982).
3. P. J. Flanders and J. P. Remeika, *Philos. Mag.* **11,** 1271 (1965); and N. A. Curry, G. B. Johnson, P. J. Besser, and A. H. Morrish, *Philos. Mag.* **12,** 221 (1965).
4. N. Yamamoto, *J. Phys. Soc. Japan* **24,** 23 (1968).
5. E. Šimánek and Ž. Sroubek, *in* "Electron Paramagnetic Resonance" (S. Geshwind, Ed.), Chap. 8, Plenum, New York/London (1972).
6. P. B. Fabritchnyi, A. M. Babechkin, and A. N. Nesmejanov, *J. Phys. Chem. Solids* **32,** 1701 (1970).
7. T. Okada, S. Ambe, F. Ambe, and H. Sekizawa, *J. Phys. Chem.* **86,** 4726 (1982).
8. E. J. Samuelson and G. Shirane, *Phys. Status Solidi* **42,** 241 (1970).
9. J. Cassedanne, *An. Acad. Bras. Cien.* **38,** 265 (1966).